


Effect of uncorrelated on-site scalar potential and mass disorder on transport of two-dimensional Dirac fermions

Arman Duha  and Mario F. Borunda ^{*}

Department of Physics, *Oklahoma State University*, Stillwater, Oklahoma 74078, USA

 (Received 11 March 2024; revised 27 July 2024; accepted 3 September 2024; published 13 September 2024)

We investigate the transport properties of massive Dirac fermions subjected to uncorrelated scalar potential disorder, and mass disorder. Using a finite difference method, the conductance is calculated for a wide variety of combinations of these two disorder strengths. By calculating the scaling of conductivity with system size we find that, depending on the combination, the system can have an insulating, scale invariant, and metallic behavior. We identify the critical values of these disorder strengths where the phase transitions occur. We study both the zero and nonzero average mass cases to examine the effect of scalar potential disorder on band gap. Our results suggest a suppression of the band gap by the scalar potential disorder.

DOI: [10.1103/PhysRevB.110.094205](https://doi.org/10.1103/PhysRevB.110.094205)

I. INTRODUCTION

Two-dimensional Dirac fermions realize a wide variety of symmetry classes when subjected to various types of disorder [1–6]. Depending on the symmetry class, phase transitions due to Anderson localization [7] vary considerably. These phase transitions include the metal-insulator transition (MIT) due to suppression of diffusion into localization and the insulator-insulator transition between separate localized phases [8–12].

Numerous studies [13–21] have looked at the phase transitions for different symmetry classes of Dirac fermion systems. Graphene [22] and chiral p -wave superconductors [23,24] are examples of some of the most studied such systems. In particular, disorder effects in transport properties are the subject of extensive investigation [25–30]. If the disorder in graphene is random scalar potential, $V(x, y)$, which breaks the chiral and particle-hole symmetry, it falls in the symmetry class AII [31]. For the chiral p -wave superconductor system with vortex disorder, chiral and time-reversal symmetry are broken, but particle-hole symmetry remains invariant, which leads the system to symmetry class BD [2]. Consequently, these two systems exhibit different types of phase transition with the variation of disorder strength.

In clean graphene, the conductivity takes a scale invariant critical value [32,33] of $\sigma_c = G_0/\pi$, where G_0 is the conductance quantum. When disorder V is introduced (Class AII), this scale invariance is known to change into logarithmic scaling of conductivity [13–15] for sufficiently strong disorder [see Fig. 1(a)]. A random mass disorder, $M(x, y) = \bar{M} + \delta M(x, y)$, can approximate a disordered chiral p -wave superconductor [17,34,35], where \bar{M} is the average mass and δM is the random mass disorder. Consequently, instead of V , if the disorder is M , the system belongs to class BD . A very different phase transition is observed for this system [17].

Depending on the disorder's strength, the system can now be at an insulating or metallic phase. This insulator-to-metal transition is marked by a critical value of disorder strength for which the conductivity is scale invariant, as indicated in Fig. 1(b).

A more general case is when both scalar potential disorder V and mass disorder M are present. In a Dirac fermion system with both V and M , all three symmetries are broken [1], which puts the system into symmetry class A [3]. Such systems have been studied extensively [1,31,36–40] and include examples such as disordered d -wave superconductor [37] and graphene on hexagonal boron nitride (h-BN) [36,41–43].

In this paper, we numerically investigate the effect of disorder on conductivity when δV and δM are simultaneously present. The physics of localization for such a system depends sensitively on the range of the disorders. Intervalley scattering is significant when short-range correlated random disorder is present, and localization sets in Refs. [13,38]. For long-range correlated disorder, the conductivity flows to the quantum Hall critical point value, $\sigma_{xx}^{\text{QHE}} \approx 0.57 \times 4e^2$, for $\bar{M} = 0$ and to zero (insulating) for $\bar{M} \neq 0$. This insulating behavior is interpreted as a band gap opening induced by, for example, the proximity of graphene to h-BN [36]. On the other hand, it has been reported that uncorrelated on-site disorder can suppress the band gap and thereby induce a metallic state [44,45]. For graphene/h-BN systems, this occurs through the on-site Coulomb impurities restoring the inversion symmetry between neighboring carbons. It has been argued that this phenomenon of band gap suppression should be present in other van der Waals heterostructures as well [44].

This paper is organized as follows. In Sec. II, we introduce the model and describe our system structure and method for calculating conductivity. We choose both types of disorders, $\delta V(x, y)$ and $\delta M(x, y)$, to be on-site and spatially uncorrelated. δV and δM are distributed uniformly in the disorder strength interval, $(-\Delta V, \Delta V)$, and $(-\Delta M, \Delta M)$, respectively. In Sec. III, we study the zero average mass ($\bar{M} = 0$) case before dealing with the nonzero average mass ($\bar{M} \neq 0$)

^{*}Contact author: mario.borunda@okstate.edu

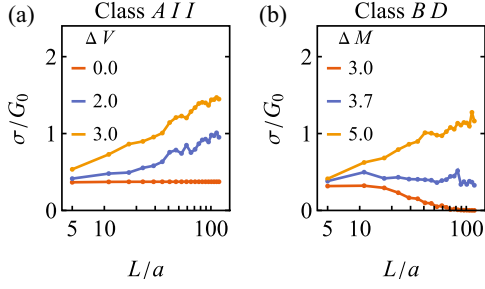


FIG. 1. Scaling of conductivity for different combinations of disorder. $\bar{M} = 0.1\hbar/va$, ΔV and ΔM are in the units of $\hbar v/a$ and \hbar/va , respectively.

in Sec. IV. Under a wide variety of disorder strengths, we calculate the change in conductivity with system size using a finite difference approximation of the transfer matrix method [15]. Our numerical results indicate that the system can behave as an insulator, scale invariant with a critical conductivity value, and a diffusive metal depending on the average mass \bar{M} and the disorder strengths. We look closer at the critical points, which separate two different phases, in Sec. V. We conclude with the summary of our results in Sec. VI.

II. MODEL

We consider here a two-dimensional massive Dirac fermion Hamiltonian that satisfies the Dirac equation

$$H\Psi = E\Psi, \quad H = v(\boldsymbol{\sigma} \cdot \mathbf{p}) + V(x, y) + v^2 M(x, y)\sigma_z, \quad (1)$$

where Ψ is the two-component spinor eigenstate, E is the energy, and v is the velocity of the Dirac fermion. The Pauli matrices ($\boldsymbol{\sigma}$) are given by the components

$$\sigma_x = \begin{pmatrix} 0 & 1 \\ 1 & 0 \end{pmatrix}, \sigma_y = \begin{pmatrix} 0 & -i \\ i & 0 \end{pmatrix}, \sigma_z = \begin{pmatrix} 1 & 0 \\ 0 & -1 \end{pmatrix}.$$

The scalar potential landscape is $V(x, y)$, and $M(x, y)$ is the local mass of the Dirac fermion. While the scalar potential V breaks the chiral and particle-hole symmetries, the Dirac mass term M breaks time-reversal symmetry, putting the system in class A.

We model disorder by having at each lattice point a random value around the Fermi energy, i.e., $V(x, y) = E + \delta V(x, y)$, where δV is the random scalar potential distributed uniformly in the interval $(-\Delta V, \Delta V)$. Similarly, a random mass fluctuation, δM , is introduced as $M(x, y) = \bar{M} + \delta M(x, y)$ distributed uniformly in the interval $(-\Delta M, \Delta M)$. Disorders are assigned randomly with a correlation length equal to the lattice constant a , illustrated in Fig. 2. These defects are realized through various physical and chemical processes. The potential model is appropriate for treating electrostatic impurities, that is, long-range impurity potentials. The transfer matrix approach used here also allows for scatterers that, although short ranged (their width being the lattice constant), do not break symplectic symmetry and thus are effectively long range. For strong δV , the method can be used to efficiently model mesoscopic systems. Any strain on the system and Coulomb impurities contribute to the scalar potential [36]. Impurities give rise to charge fluctuations in charge density, Δn ,

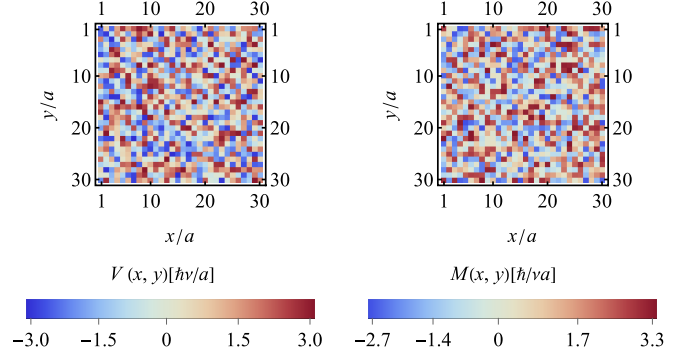


FIG. 2. On-site random scalar potential $V(x, y) = \delta V$ (left) and random mass $M(x, y) = \bar{M} + \delta M$ (right). $\bar{M} = 0.3\hbar/va$ and disorder strengths are $\Delta V = 3\hbar v/a$, $\Delta M = 3\hbar/va$.

that are related to fluctuations in potential by $\Delta V = \hbar v \sqrt{\pi \Delta n}$ [46]. For graphene, typical values of charge fluctuation range from $\Delta n = 10^{10} - 10^{12} \text{ cm}^{-2}$. Assuming that the lattice constant used when discretizing the system uses a lattice constant of $a = 30 \text{ nm}$, the range of fluctuations corresponds to $\Delta V = [0.5 - 5.5] \hbar v/a = [12 - 123] \text{ meV}$.

For multilayer systems, unprecedented precision of twist angle and interlayer distance [47–50] has made it possible to control the interlayer coupling, which strongly affects the electronic structure and can result in a gap opening [51–54], which corresponds to the average mass \bar{M} . For twisted graphene/h-BN heterostructure, experiments report a band gap opening that ranges from 2–14 meV depending on the twist angle between graphene and h-BN [55]. The disorder strength ΔM can be varied by tuning the gate voltage, V_r . A particular ΔM is obtained from a fixed V_r and the randomness comes from the fact that in a realistic system, V_r is not uniform along the graphene sheet, resulting in a random $M(x, y)$ in the Hamiltonian (1) [56]. Throughout this paper, we work with various mass disorders up to a maximum value of $\Delta M = 12 \hbar/va$, which corresponds to tuning a gate voltage of $V_r = 275 \text{ meV}$.

In our calculations, we model the system around the Dirac point, $V = \delta V$. We consider four different values of average mass, \bar{M} , including the zero average mass case for benchmarking our results. The disorders, δV and δM are assigned at each lattice point independently from its neighboring lattice points, i.e., correlation length is equal to the lattice constant.

We find the conductance of the system by mapping the Hamiltonian to a finite difference method (see Ref. [15] for details) for solving the scattering by disorder problem of Dirac fermions. Our approach is the so-called staggered-fermion model, initially developed in lattice gauge theory [57,58], extensively used for calculating conductivity of different Dirac fermion systems [15–18,59–62].

The geometry of the two-dimensional system we consider is of length $L = N_x a$ and width $W = N_y a$. The microscopic details of the transverse edge states and the boundary condition become irrelevant in the large aspect ratio $W/L \gg 1$. It has been shown that for an aspect ratio of $W/L = 3$, the conductivity already reaches the $W/L = \infty$ limit [15,32]. In this work all calculations assume periodic boundary conditions along the transverse direction with the system

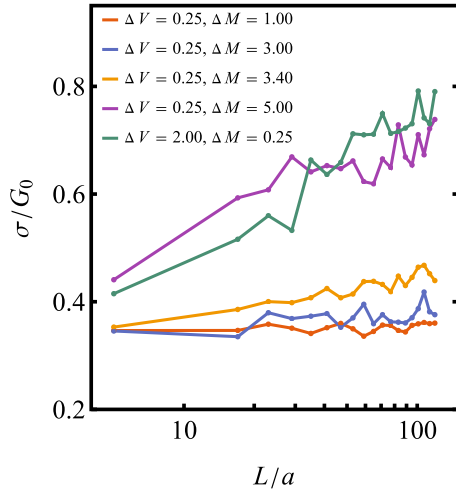


FIG. 3. Scaling of conductivity behavior for solo disorder (either ΔV or ΔM) is recovered in the presence of dual disorder (ΔV and ΔM) for vanishing value of one.

having an aspect ratio of $W/L = 3$. The Hamiltonian and the boundary conditions are used to write the transfer matrix \mathcal{T} . The derivation of the transfer matrix \mathcal{T} is presented in the Appendix for completeness. The transmission matrix T was calculated from the evolution of eigenstates from one end of the system to the other via the transfer matrix. The conductance is calculated using the Landauer formula

$$G = G_0 \sum_n T_n, \quad (2)$$

where G_0 is the conductance quantum and T_n are the eigenvalues of the transmission matrix T . $\langle G \rangle$ is the average of the conductance taken over many disorder realizations and is used to calculate the average conductivity, $\sigma = (L/W)\langle G \rangle$.

III. ZERO AVERAGE MASS ($\bar{M} = 0$)

The scaling behavior of conductivity in the presence of one type of disorder (either scalar potential or mass) while the other type is absent is well known [15,17,34,35,63–65]. To investigate the combined effect of the two disorders, we start with two limiting cases, i.e., small mass fluctuations ($\Delta M \approx 0$) with $\Delta V > 0$, and small potential fluctuations ($\Delta V \approx 0$) with $\Delta M > 0$. For small ΔM and nonzero ΔV , the conductivity scales towards that of a diffusive metal, as shown by the green line in Fig. 3. These results agree with Ref. [15].

On the other hand, for small ΔV and nonzero ΔM , two phases are observed at $\bar{M} = 0$ [8,9], separated by a tricritical point, ΔM^* [17]. The tricritical point is defined as the value of mass disorder such that for $\Delta M < \Delta M^*$ the system approaches the scale invariant critical conductivity and $\Delta M > \Delta M^*$ drives the system to a diffusive metal phase. We identify this behavior in Fig. 3 for a small ΔV ($= 0.25 \hbar v/a$). The system is driven to a diffusive metal phase around $\Delta M^* \approx 3.2 \hbar v/a$ and remains metallic for still higher values of ΔM . This result agrees with previous numerical results [17,64,65] found for the $\Delta V = 0$ case.

In Fig. 4, we present the phase diagram by numerically calculating ΔM^* for different ΔV values. ΔM^* decreases

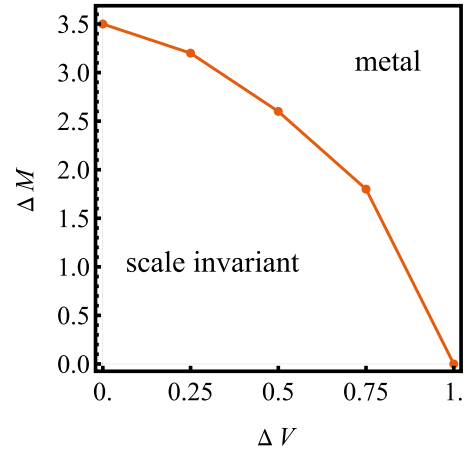


FIG. 4. Phase diagram for the $\bar{M} = 0$ case. Data points are the critical mass disorder values, ΔM^* , that separate the scale invariant phase from the metallic phase at the corresponding ΔV .

with increasing ΔV and eventually becomes zero. We define this value of ΔV , for which ΔM^* reaches zero, as the critical scalar potential disorder, ΔV^* . for $\Delta V > \Delta V^*$, the system loses access to the scale invariant phase and must remain metallic regardless of the ΔM value. For the massless case here, $\Delta V^* = 1 \hbar v/a$, and as we will see in the next section, ΔV^* increases with increasing average mass \bar{M} .

We now consider the case when both ΔV and ΔM are comparable in strength. We consider a wide range of ΔM values for two fixed values of ΔV to examine the conductivity under their combined effect.

Similar to the lone ΔV disorder case, the conductivity always increases logarithmically with system size L . This increase occurs regardless of the disorder strength ΔM . However, compared to the lone ΔV case, the conductivity curve is significantly flattened, i.e., conductivity increases much slower with system size when ΔV and ΔM are present simultaneously.

Figure 5 also indicates that increasing ΔM initially decreases the overall conductivity, presumably due to some competing effect between ΔV and ΔM . However, after reaching a minimum value, the conductivity increases with ΔM . This increase occurs only when ΔM is large enough to be

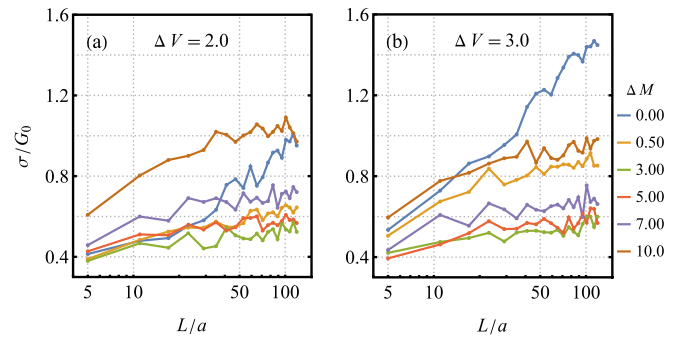


FIG. 5. Scaling of conductivity σ for different ΔM at $\bar{M} = 0$. Two ΔV cases are demonstrated for both of which σ starts decreasing at first with increasing ΔM and reaches a minimum value before increasing with ΔM .

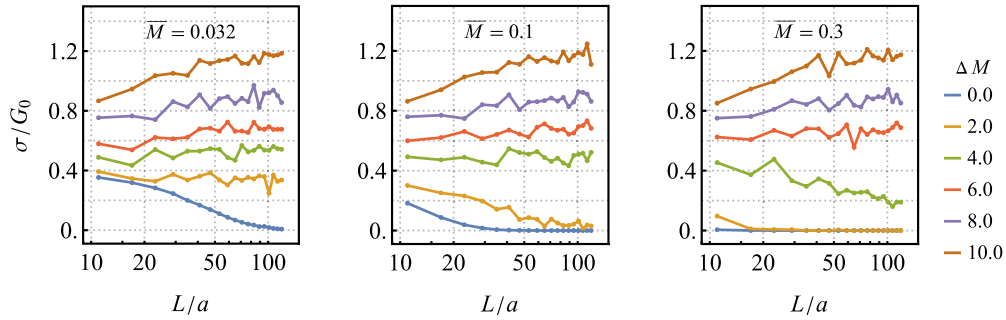


FIG. 6. Scaling of conductivity σ for different ΔM in the $\Delta V < \Delta V^*$ case. The system exhibits insulating, scale invariant, and metallic behavior. ΔM^* increases with increasing \bar{M} . In all three cases $\Delta V = 1 \hbar v/a$.

the dominant disorder such that it increases the conductivity, much like when ΔM is the only disorder.

IV. NONZERO AVERAGE MASS ($\bar{M} \neq 0$)

So far, we have considered the zero average Dirac mass case ($\bar{M} = 0$). We now examine the nonzero \bar{M} case in the presence of ΔV and ΔM . We work with three average masses: $\bar{M} = 0.032, 0.1$, and $0.3 \hbar/va$. For graphene/h-BN with a twist angle $\theta > 1$, the band gap Δ_g varies from 2–6 meV and a maximum band gap of 14 meV is observed for near $\theta = 0$ alignment [55]. For a puddle size of $a = 30$ nm, our choice of $\bar{M} = 0.032 \hbar/va$ ($\Delta_g = 2$ meV), and $\bar{M} = 0.1 \hbar/va$ ($\Delta_g = 5$ meV) corresponds to the $\theta > 1$ alignment, and $\bar{M} = 0.3 \hbar/va$ ($\Delta_g = 14$ meV) corresponds to the $\theta = 0$ alignment. For correlated disorder, a nonzero \bar{M} is known to drive the system to an insulator. We also identify such an insulating phase for uncorrelated ΔM , but this phase is now controlled by both ΔV and ΔM . Only for ΔV and ΔM values smaller than particular critical values, ΔV^* and ΔM^* , does the insulating phase exist. We discuss these critical values in Sec. V.

When $\Delta V < \Delta V^*$, various conductivity scaling behaviors are observed. Figure 6 shows that as we increase the ΔM values, the system switches from insulating to a scale invariant conductivity and finally to a metallic phase. We identify the ΔM value at which the system transitions from insulating behavior to scale invariant conductivity as the critical mass disorder $\equiv \Delta M^*$. This critical value depends on \bar{M} and ΔV . If the system's average mass \bar{M} increases, so does the required mass disorder, ΔM^* , to lift the system from the insulating phase. However, once the system reaches the metallic phase at ΔM values higher than its corresponding ΔM^* , the conductivity scaling remains the same for different \bar{M} values, as seen in Fig. 6.

There is no insulating phase for $\Delta V > \Delta V^*$. The variation of conductivity scaling with ΔM is similar to that of the $\bar{M} = 0$ case. In other words, the band gap (\bar{M}) is suppressed by introducing ΔV , and for a sufficiently strong value, the conductivity is much like the closed band ($\bar{M} = 0$) case. This is indicated in Fig. 7, which shows that, like the $\bar{M} = 0$ case, conductivity first decreases with ΔM and reaches a minimum value before increasing with larger values of ΔM . This result agrees with the results found in Refs. [44,45] that the band gap is suppressed by uncorrelated on-site scalar potential.

V. CRITICAL POINTS

In Sec. IV, the transitions of scaling behavior (from insulating to scale invariant and metallic) are demonstrated without specifying the transition points. We now focus on numerically evaluating the critical points, ΔV^* and ΔM^* , at which these transitions occur. As mentioned, the insulating phase can only exist for ΔV values below a critical value, ΔV^* . We interpret ΔV^* as the onsite potential disorder width necessary for quelling the band gap to zero. ΔV^* thus depends on \bar{M} (band gap), i.e., $\Delta V^* = \Delta V^*(\bar{M})$. In Fig. 8, we identify the $\Delta V^*(\bar{M})$ values by calculating the scale dependence of conductivity for different ΔV at $\Delta M = 0$. As expected, a more significant value of \bar{M} requires a larger ΔV^* to change the conductivity scaling from insulating to scale invariant. Fitting our data gives the relationship, $\Delta V^* = 17.12\bar{M}^{1.44} + 1.48$, which shows a power-law dependency of ΔV^* on the band gap \bar{M} .

The critical scalar potential disorder strength, ΔV^* , acts as a boundary above which the insulating phase disappears, but for $\Delta V < \Delta V^*$, the system can have all three scaling behaviors. Precisely which scale dependence the system will exhibit for a particular ΔV depends on the value of the mass disorder strength, ΔM . We illustrate this dependence in Fig. 6 where we notice that the system is insulating for $\Delta M = 0$ and reaches a scale invariant conductivity as we increase ΔM . We identify the ΔM^* values by calculating the scale dependence of conductivity for three different \bar{M} values, as shown in Fig. 9 for $\Delta V = 1 \hbar v/a$. The required ΔM^* values increase logarithmically with \bar{M} according to the relationship $\Delta M^* = 0.56 \ln[\bar{M} - 0.03] + 5.48$ obtained by fitting our data. Similarly, we have calculated the ΔM^* values for several ΔV in the range 0 to ΔV^* . This allows us to look at the phase diagram (similar to Fig. 4) for the $\bar{M} \neq 0$ case. We note that the phase boundary in this phase diagram, shown in Fig. 10, differs from the phase boundary of $\bar{M} = 0$ case, which separated the scale invariant from metallic phase. For the $\bar{M} \neq 0$ case, the phase boundary now separates the insulating phase from the scale invariant.

After reaching the scale invariant conductivity at $\Delta M = \Delta M^*$, the conductivity increase with system size for ΔM values larger than ΔM^* is relatively slow. This trend is shown in Fig. 6. It is part of the general observation that when ΔV and ΔM are of comparable strength, and the system is in a metallic phase, the system is a poor conductor because the

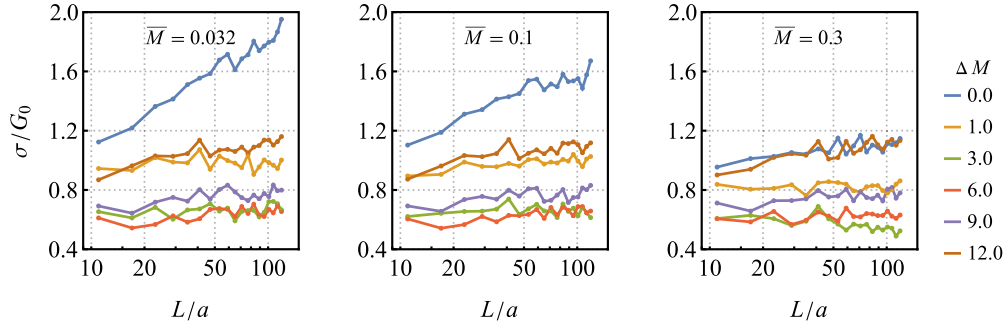


FIG. 7. Scaling of conductivity σ for different ΔM in the $\Delta V > \Delta V^*$ case. The system no longer exhibits insulating behavior. Similar to the $\bar{M} = 0$ case, σ starts decreasing at first with increasing ΔM and reaches a minimum value before increasing with increasing ΔM . In all three cases $\Delta V = 5 \hbar v/a$.

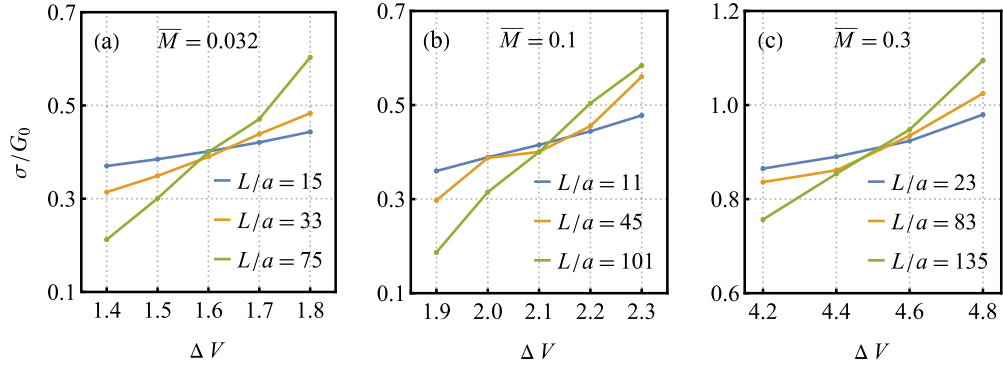


FIG. 8. Change of conductivity σ with ΔV . ΔV^* is calculated by identifying the value of ΔV at which the conductivity becomes scale invariant. The required ΔV^* value increases with \bar{M} .

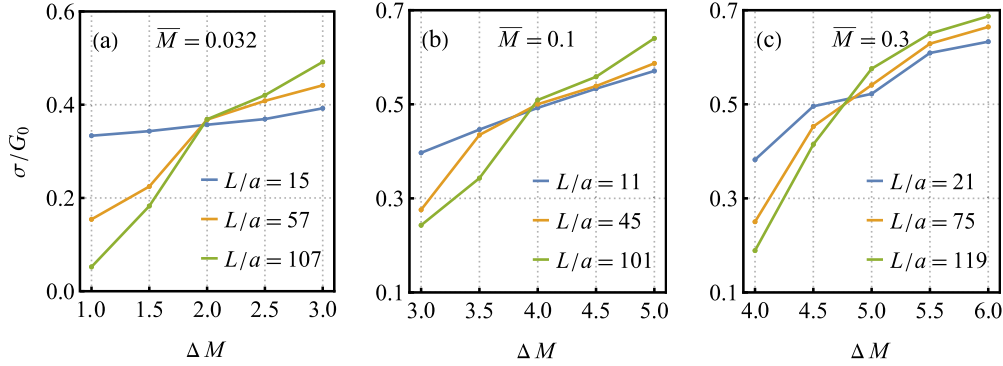


FIG. 9. Change of conductivity σ with ΔM . ΔM^* is calculated by identifying the value of ΔM at which the conductivity becomes scale invariant. ΔV is fixed at $\Delta V = 1 \hbar v/a$.

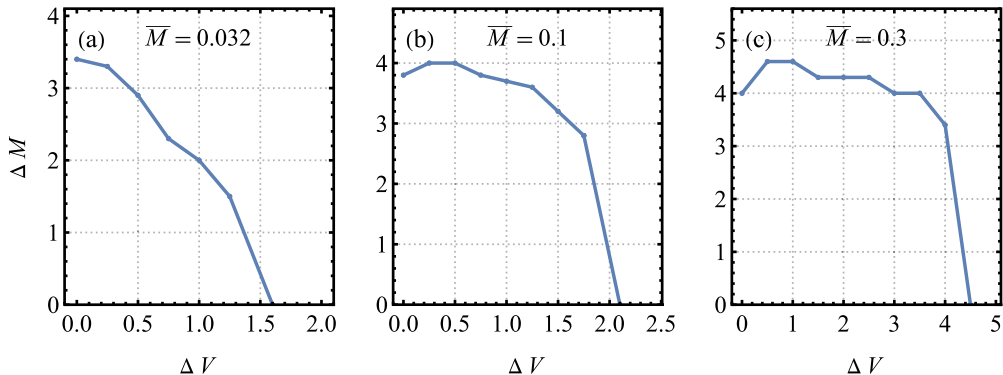


FIG. 10. Phase diagram for the $\bar{M} \neq 0$ case. Data points are the critical mass disorder values, ΔM^* , below which the system remains in insulating phase at the corresponding ΔV .

conductivity increase rate with system size L is sluggish. This is also seen in Fig. 7 where we notice that the conductivity is lowest and has the flattest scaling when the disorder strengths ΔV and ΔM are similar.

VI. CONCLUSION

In this paper, we have studied the transport properties of a massive Dirac fermion in the simultaneous presence of scalar potential disorder ΔV and mass disorder ΔM . Our numerical calculations use the real space tight-binding model on a lattice with on-site uncorrelated disorder developed by Tworzydło *et al.* [15,17]. We study three different average masses, \bar{M} , which is interpreted as the band gap. In all three cases, despite the band gap, we identify that a critical $\Delta V^*(\bar{M})$ exists above which the system can no longer be an insulator for any ΔM . The results support the idea of band gap suppression by on-site Coulomb potential in the analytical calculations discussed in Refs. [44,45]. For $\Delta V < \Delta V^*$, the system can be in an insulating or metallic phase, depending on the ΔM value. As ΔM increases, the system exhibits an insulator-to-metal transition at a critical value $\Delta M^*(\bar{M}, \Delta V)$. We have numerically estimated the critical values, ΔV^* , and ΔM^* , for different \bar{M} values. Our work demonstrates the interdependent way different types of disorders can affect the phases accessible to a massive Dirac fermion system.

ACKNOWLEDGMENTS

The calculations were performed in the PETE system of the High Performance Computing Center at Oklahoma State University, NSF Grant No. OAC-1531128.

APPENDIX: TRANSFER MATRIX

The Dirac equation given in Eq. (1) can be rearranged as,

$$\partial_x \Psi = \left(-i\sigma_z \partial_y - i\sigma_x \frac{V}{\hbar v} - \frac{vM}{\hbar} \sigma_y \right) \Psi.$$

Using the discretization method of Ref. [15], the discretized Dirac equation is expressed by

$$\begin{aligned} & \frac{1}{2a} \mathcal{J}(\Psi_{m+1} - \Psi_m) \\ &= \left(-\frac{i}{2a} \sigma_z \mathcal{K} - \frac{i}{4\hbar v} \sigma_x \mathcal{V}^{(m)} - \frac{v}{4\hbar} \sigma_y \mathcal{M}^{(m)} \right) (\Psi_m + \Psi_{m+1}), \end{aligned}$$

where \mathcal{J} , \mathcal{K} , $\mathcal{V}^{(m)}$, and $\mathcal{M}^{(m)}$ are matrices with the following nonzero elements:

$$\begin{aligned} \mathcal{J}_{n,n} &= 1, & \mathcal{J}_{n,n+1} &= \mathcal{J}_{n,n-1} = \frac{1}{2}, \\ \mathcal{K}_{n,n+1} &= \frac{1}{2}, & \mathcal{K}_{n,n-1} &= -\frac{1}{2}, \\ \mathcal{V}_{n,n}^{(m)} &= \frac{1}{2}(V_{m,n} + V_{m,n-1}), & \mathcal{V}_{n,n+1}^{(m)} &= \frac{1}{2}V_{m,n}, \\ \mathcal{V}_{n,n-1}^{(m)} &= \frac{1}{2}V_{m,n-1}, \\ \mathcal{M}_{n,n}^{(m)} &= \frac{1}{2}(M_{m,n} + M_{m,n-1}), & \mathcal{M}_{n,n+1}^{(m)} &= \frac{1}{2}M_{m,n}, \\ \mathcal{M}_{n,n-1}^{(m)} &= \frac{1}{2}M_{m,n-1}. \end{aligned}$$

The transfer matrix, \mathcal{T}_m , which is defined as,

$$\Psi_{m+1} = \mathcal{T}_m \Psi_m$$

is then given by

$$\mathcal{T}_m = \frac{(\mathcal{J} - i\sigma_z \mathcal{K} - \frac{a}{2\hbar v} i\sigma_x \mathcal{V}^{(m)} - \frac{va}{2\hbar} \sigma_y \mathcal{M}^{(m)})}{(\mathcal{J} + i\sigma_z \mathcal{K} + \frac{a}{2\hbar v} i\sigma_x \mathcal{V}^{(m)} + \frac{va}{2\hbar} \sigma_y \mathcal{M}^{(m)})}.$$

-
- [1] A. W. W. Ludwig, M. P. A. Fisher, R. Shankar, and G. Grinstein, Integer quantum Hall transition: An alternative approach and exact results, *Phys. Rev. B* **50**, 7526 (1994).
 - [2] M. Bocquet, D. Serban, and M. Zirnbauer, Disordered 2d quasiparticles in class D: Dirac fermions with random mass, and dirty superconductors, *Nucl. Phys. B* **578**, 628 (2000).
 - [3] D. Bernard and A. LeClair, A classification of 2D random Dirac fermions, *J. Phys. A* **35**, 2555 (2002).
 - [4] F. Evers and A. D. Mirlin, Anderson transitions, *Rev. Mod. Phys.* **80**, 1355 (2008).
 - [5] S. Ryu, A. P. Schnyder, A. Furusaki, and A. W. Ludwig, Topological insulators and superconductors: Tenfold way and dimensional hierarchy, *New J. Phys.* **12**, 065010 (2010).
 - [6] A. Altland and M. R. Zirnbauer, Nonstandard symmetry classes in mesoscopic normal-superconducting hybrid structures, *Phys. Rev. B* **55**, 1142 (1997).
 - [7] P. W. Anderson, Absence of diffusion in certain random lattices, *Phys. Rev.* **109**, 1492 (1958).
 - [8] J. T. Chalker, N. Read, V. Kagalovsky, B. Horovitz, Y. Avishai, and A. W. W. Ludwig, Thermal metal in network models of a disordered two-dimensional superconductor, *Phys. Rev. B* **65**, 012506 (2001).
 - [9] V. Kagalovsky and D. Nemirovsky, Universal critical exponent in class d superconductors, *Phys. Rev. Lett.* **101**, 127001 (2008).
 - [10] L. Ponomarenko, A. Geim, A. Zhukov, R. Jalil, S. Morozov, K. Novoselov, I. Grigorieva, E. Hill, V. Cheianov, V. Fal'ko *et al.*, Tunable metal-insulator transition in double-layer graphene heterostructures, *Nat. Phys.* **7**, 958 (2011).
 - [11] E. J. König, P. M. Ostrovsky, I. V. Protopopov, and A. D. Mirlin, Metal-insulator transition in two-dimensional random fermion systems of chiral symmetry classes, *Phys. Rev. B* **85**, 195130 (2012).
 - [12] J. F. Karcher, I. A. Gruzberg, and A. D. Mirlin, Generalized multifractality at metal-insulator transitions and in metallic phases of two-dimensional disordered systems, *Phys. Rev. B* **106**, 104202 (2022).
 - [13] K. Nomura, M. Koshino, and S. Ryu, Topological delocalization of two-dimensional massless Dirac fermions, *Phys. Rev. Lett.* **99**, 146806 (2007).
 - [14] J. H. Bardarson, J. Tworzydło, P. W. Brouwer, and C. W. J. Beenakker, One-parameter scaling at the Dirac point in graphene, *Phys. Rev. Lett.* **99**, 106801 (2007).
 - [15] J. Tworzydło, C. W. Groth, and C. W. J. Beenakker, Finite difference method for transport properties of massless Dirac fermions, *Phys. Rev. B* **78**, 235438 (2008).

- [16] J. H. Bardarson, M. V. Medvedyeva, J. Tworzydło, A. R. Akhmerov, and C. W. J. Beenakker, Absence of a metallic phase in charge-neutral graphene with a random gap, *Phys. Rev. B* **81**, 121414(R) (2010).
- [17] M. V. Medvedyeva, J. Tworzydło, and C. W. J. Beenakker, Effective mass and tricritical point for lattice fermions localized by a random mass, *Phys. Rev. B* **81**, 214203 (2010).
- [18] M. V. Medvedyeva, On localization of Dirac fermions by disorder, Ph.D. thesis, Leiden University, 2011.
- [19] A. Schuessler, P. M. Ostrovsky, I. V. Gornyi, and A. D. Mirlin, Analytic theory of ballistic transport in disordered graphene, *Phys. Rev. B* **79**, 075405 (2009).
- [20] B. Lian, J. Wang, X.-Q. Sun, A. Vaezi, and S.-C. Zhang, Quantum phase transition of chiral majorana fermions in the presence of disorder, *Phys. Rev. B* **97**, 125408 (2018).
- [21] X. Luo, Z. Xiao, K. Kawabata, T. Ohtsuki, and R. Shindou, Unifying the anderson transitions in hermitian and non-Hermitian systems, *Phys. Rev. Res.* **4**, L022035 (2022).
- [22] A. K. Geim and K. S. Novoselov, The rise of graphene, *Nat. Mater.* **6**, 183 (2007).
- [23] C. Kallin and A. Berlinsky, Is Sr_2RuO_4 a chiral p-wave superconductor? *J. Phys.: Condens. Matter* **21**, 164210 (2009).
- [24] S. Tewari, S. Das Sarma, C. Nayak, C. Zhang, and P. Zoller, Quantum computation using vortices and majorana zero modes of a $p_x + ip_y$ superfluid of fermionic cold atoms, *Phys. Rev. Lett.* **98**, 010506 (2007).
- [25] Y. Chen, B. Fu, J. Xu, Q. Shi, P. Cui, and Z. Zhang, Quasiparticle and transport properties of disordered bilayer graphene, *Phys. Rev. B* **108**, 064208 (2023).
- [26] B. Fu, Y. Chen, W. Chen, W. Zhu, P. Cui, Q. Li, Z. Zhang, and Q. Shi, Disorder effects on the quasiparticle and transport properties of two-dimensional dirac fermionic systems, *Phys. Rev. B* **108**, 064207 (2023).
- [27] F. Anwar, A. Iurov, D. Huang, G. Gumbs, and A. Sharma, Interplay between effects of barrier tilting and scatterers within a barrier on tunneling transport of dirac electrons in graphene, *Phys. Rev. B* **101**, 115424 (2020).
- [28] N. J. G. Couto, D. Costanzo, S. Engels, D.-K. Ki, K. Watanabe, T. Taniguchi, C. Stampfer, F. Guinea, and A. F. Morpurgo, Random strain fluctuations as dominant disorder source for high-quality on-substrate graphene devices, *Phys. Rev. X* **4**, 041019 (2014).
- [29] J. Meng, R. Mondaini, T. Ma, and H.-Q. Lin, Inducing a metal-insulator transition in disordered interacting dirac fermion systems via an external magnetic field, *Phys. Rev. B* **104**, 045138 (2021).
- [30] A. Hui, S. Lederer, V. Oganessian, and E.-A. Kim, Quantum aspects of hydrodynamic transport from weak electron-impurity scattering, *Phys. Rev. B* **101**, 121107(R) (2020).
- [31] P. M. Ostrovsky, I. V. Gornyi, and A. D. Mirlin, Quantum criticality and minimal conductivity in graphene with long-range disorder, *Phys. Rev. Lett.* **98**, 256801 (2007).
- [32] J. Tworzydło, B. Trauzettel, M. Titov, A. Rycerz, and C. W. J. Beenakker, Sub-poissonian shot noise in graphene, *Phys. Rev. Lett.* **96**, 246802 (2006).
- [33] M. Katsnelson, Zitterbewegung, chirality, and minimal conductivity in graphene, *Eur. Phys. J. B* **51**, 157 (2006).
- [34] T. Wang, Z. Pan, T. Ohtsuki, I. A. Gruzberg, and R. Shindou, Multicriticality of two-dimensional class-D disordered topological superconductors, *Phys. Rev. B* **104**, 184201 (2021).
- [35] Z. Pan, T. Wang, T. Ohtsuki, and R. Shindou, Renormalization group analysis of dirac fermions with a random mass, *Phys. Rev. B* **104**, 174205 (2021).
- [36] M. Titov and M. I. Katsnelson, Metal-insulator transition in graphene on boron nitride, *Phys. Rev. Lett.* **113**, 096801 (2014).
- [37] A. Altland, B. Simons, and M. Zirnbauer, Theories of low-energy quasi-particle states in disordered D-wave superconductors, *Phys. Rep.* **359**, 283 (2002).
- [38] K. Nomura, S. Ryu, M. Koshino, C. Mudry, and A. Furusaki, Quantum Hall effect of massless dirac fermions in a vanishing magnetic field, *Phys. Rev. Lett.* **100**, 246806 (2008).
- [39] A. Hill and K. Ziegler, Scaling behavior of disordered lattice fermions in two dimensions, *Eur. Phys. J. B* **87**, 142 (2014).
- [40] B. Sierski, E. J. Dresselhaus, J. E. Moore, and I. A. Gruzberg, Criticality of two-dimensional disordered dirac fermions in the unitary class and universality of the integer quantum Hall transition, *Phys. Rev. Lett.* **126**, 076801 (2021).
- [41] R. Decker, Y. Wang, V. W. Brar, W. Regan, H.-Z. Tsai, Q. Wu, W. Gannett, A. Zettl, and M. F. Crommie, Local electronic properties of graphene on a BN substrate via scanning tunneling microscopy, *Nano Lett.* **11**, 2291 (2011).
- [42] C. R. Dean, A. F. Young, I. Meric, C. Lee, L. Wang, S. Sorgenfrei, K. Watanabe, T. Taniguchi, P. Kim, K. L. Shepard *et al.*, Boron nitride substrates for high-quality graphene electronics, *Nat. Nanotechnol.* **5**, 722 (2010).
- [43] R. Martinez-Gordillo, S. Roche, F. Ortmann, and M. Pruneda, Transport fingerprints at graphene superlattice dirac points induced by a boron nitride substrate, *Phys. Rev. B* **89**, 161401(R) (2014).
- [44] J.-R. Xu, Z.-Y. Song, C.-G. Yuan, and Y.-Z. Zhang, Interaction-induced metallic state in graphene on hexagonal boron nitride, *Phys. Rev. B* **94**, 195103 (2016).
- [45] X. Li, L. Xu, and J. Zhang, Band structure and transport property of graphene/h-BN heterostructure under local potentials, *Chin. J. Phys.* **65**, 75 (2020).
- [46] A. Deshpande, W. Bao, Z. Zhao, C. N. Lau, and B. J. LeRoy, Imaging charge density fluctuations in graphene using coulomb blockade spectroscopy, *Phys. Rev. B* **83**, 155409 (2011).
- [47] M. Liao, Z. Wei, L. Du, Q. Wang, J. Tang, H. Yu, F. Wu, J. Zhao, X. Xu, B. Han *et al.*, Precise control of the interlayer twist angle in large scale MoS_2 homostructures, *Nature Commun.* **11**, 2153 (2020).
- [48] P. Solís-Fernández, Y. Terao, K. Kawahara, W. Nishiyama, T. Uwanoo, Y.-C. Lin, K. Yamamoto, H. Nakashima, K. Nagashio, H. Hibino, K. Suenaga, and H. Ago, Isothermal growth and stacking evolution in highly uniform bernal-stacked bilayer graphene, *ACS Nano* **14**, 6834 (2020).
- [49] M. Brzhezinskaya, O. Kononenko, V. Matveev, A. Zotov, I. I. Khodos, V. Levashov, V. Volkov, S. I. Bozhko, S. V. Chekmazov, and D. Roshchupkin, Engineering of numerous moiré superlattices in twisted multilayer graphene for twistronics and straintronics applications, *ACS Nano* **15**, 12358 (2021).
- [50] A. Uri, S. C. de la Barrera, M. T. Randeria, D. Rodan-Legrain, T. Devakul, P. J. Crowley, N. Paul, K. Watanabe, T. Taniguchi, R. Lifshitz *et al.*, Superconductivity and strong interactions in a tunable moiré quasicrystal, *Nature (London)* **620**, 762 (2023).
- [51] E. Wang, X. Lu, S. Ding, W. Yao, M. Yan, G. Wan, K. Deng, S. Wang, G. Chen, L. Ma *et al.*, Gaps induced by inversion symmetry breaking and second-generation dirac cones in graphene/hexagonal boron nitride, *Nat. Phys.* **12**, 1111 (2016).

- [52] A. Kerelsky, L. J. McGilly, D. M. Kennes, L. Xian, M. Yankowitz, S. Chen, K. Watanabe, T. Taniguchi, J. Hone, C. Dean *et al.*, Maximized electron interactions at the magic angle in twisted bilayer graphene, *Nature (London)* **572**, 95 (2019).
- [53] C. Ghosal, M. Gruschwitz, J. Koch, S. Gemming, and C. Tegenkamp, Proximity-induced gap opening by twisted plumbene in epitaxial graphene, *Phys. Rev. Lett.* **129**, 116802 (2022).
- [54] J. Shi, J. Zhu, and A. H. MacDonald, Moiré commensurability and the quantum anomalous hall effect in twisted bilayer graphene on hexagonal boron nitride, *Phys. Rev. B* **103**, 075122 (2021).
- [55] T. Han, J. Yang, Q. Zhang, L. Wang, K. Watanabe, T. Taniguchi, P. L. McEuen, and L. Ju, Accurate measurement of the gap of Graphene/ h -BN moiré superlattice through photocurrent spectroscopy, *Phys. Rev. Lett.* **126**, 146402 (2021).
- [56] B. Dora and K. Ziegler, Gaps and tails in graphene and graphane, *New J. Phys.* **11**, 095006 (2009).
- [57] R. Stacey, Eliminating lattice fermion doubling, *Phys. Rev. D* **26**, 468 (1982).
- [58] C. M. Bender, K. A. Milton, and D. H. Sharp, Consistent formulation of fermions on a minkowski lattice, *Phys. Rev. Lett.* **51**, 1815 (1983).
- [59] M. F. Borunda, J. Berezovsky, R. M. Westervelt, and E. J. Heller, Imaging universal conductance fluctuations in graphene, *ACS Nano* **5**, 3622 (2011).
- [60] M. F. Borunda, H. Hennig, and E. J. Heller, Ballistic versus diffusive transport in graphene, *Phys. Rev. B* **88**, 125415 (2013).
- [61] C. Beenakker, A. Donís Vela, G. Lemut, M. Pacholski, and J. Tworzydło, Tangent fermions: Dirac or majorana fermions on a lattice without fermion doubling, *Ann. Phys. (N.Y.)*, **535** 2300081 (2023).
- [62] M. Pacholski, G. Lemut, J. Tworzydło, and C. Beenakker, Generalized eigenproblem without fermion doubling for dirac fermions on a lattice, *SciPost Phys.* **11**, 105 (2021).
- [63] D. Abergel, V. Apalkov, J. Berashevich, K. Ziegler, and T. Chakraborty, Properties of graphene: A theoretical perspective, *Adv. Phys.* **59**, 261 (2010).
- [64] K. Ziegler, Random-gap model for graphene and graphene bilayers, *Phys. Rev. Lett.* **102**, 126802 (2009).
- [65] K. Ziegler and A. Sinner, Transport in finite graphene samples with a random gap, *Phys. Rev. B* **81**, 241404(R) (2010).